Partial bosonization for the two-dimensional Hubbard model

Tobias Denz,[1] Mario Mitter,[1] Jan M. Pawlowski,[1,2] Christof Wetterich,[1] and Masatoshi Yamada[1]
[1]*Institut für Theoretische Physik, Universität Heidelberg, Philosophenweg 16, 69120 Heidelberg, Germany*
[2]*ExtreMe Matter Institute EMMI, GSI Helmholtzzentrum für Schwerionenforschung mbH, Planckstr. 1, 64291 Darmstadt, Germany*

(Received 25 October 2019; accepted 20 March 2020; published 14 April 2020)

Partial bosonization of the two-dimensional Hubbard model focuses the functional renormalization flow on channels in which interactions become strong and local order sets in. We compare the momentum structure of the four-fermion vertex, obtained on the basis of a patching approximation, to an effective bosonic description. For parameters in the antiferromagnetic phase near the onset of local antiferromagnetic order, the interaction of the electrons is indeed well described by the exchange of collective bosonic degrees of freedom. The residual four-fermion vertex after the subtraction of the bosonic-exchange contribution is small. We propose that similar partial bosonization techniques can improve the accuracy of renormalization flow studies also for the case of competing order.

DOI: 10.1103/PhysRevB.101.155115

I. INTRODUCTION

Cuprates exhibiting high-T_C superconductivity [1,2] feature effectively two-dimensional CuO_2 layers. For this reason, Anderson [3], as well as Zhang and Rice [4], proposed using the two-dimensional Hubbard model on a square lattice [5–7] to describe the phase diagram of these superconductors. Despite the Hubbard model's conceptual simplicity, only a few features are known rigorously for special cases [8]. A quantitative understanding of the macroscopic properties of this simple microscopic model has remained a great challenge for theoretical many-body physics. In particular, it is expected that competing order effects of the strongly correlated fermions lead to a particularly rich phase structure.

Functional renormalization group (FRG) techniques have already made important contributions [9–49] to a qualitative and sometimes quantitative understanding of the two-dimensional Hubbard model on a square lattice. For a computation of the phase structure of the Hubbard model it is crucial to precisely take into account fluctuations beyond the mean-field approximation. Because of its nonperturbative and versatile character, it is expected that the FRG is well suited to capture the relevant dynamics. In parallel, numerical simulations based on the Monte Carlo method have provided first-principles computations for such strongly correlated systems [50–58]. It is difficult, however, to use them to investigate the full phase structure of the Hubbard model due to the sign problem in systems with a finite chemical potential. Furthermore, diagrammatic resummation techniques as dynamical mean-field theory (DMFT) have provided insight into important structures of the Hubbard model [59–61]. They can be combined with FRG, called DMF^{2}RG [62]. (For a compilation, see [63] and references therein.)

The Hubbard model is defined as a purely fermionic model which describes the hopping and scattering of electrons on a lattice. It provides a natural description of the relevant microscopic electron dynamics in solids. On the other hand, the macroscopic properties, reflected in various possible order parameters, and long-range dynamics, are most easily described by collective bosonic excitations such as antiferromagnetic spin waves or d-wave electron pairs. Order parameters can be interpreted as the expectation values of these composite bosonic fields.

Within the FRG, two main approaches have been followed. The first concentrates on the flow of the four-fermion interaction in a purely fermionic setting. On microscopic scales, one starts with a pointlike interaction. As more and more fluctuations are included, the renormalization flow generates a complicated momentum dependence of this vertex. Following numerically the flow of the momentum-dependent interaction, one observes strong enhancements, and even divergences, in certain momentum channels. This is related to the possible onset of condensation phenomena in the corresponding channels. First set up for a description of collective mesons in a purely fermionic quark model [64], this method has found important developments for strongly correlated electrons. In particular, the N-patching method [14] has allowed for a better resolution of the momentum dependence of the four-fermion coupling and provided many insights for the Hubbard model [14–17], and other strongly correlated electron systems like, e.g., pnictides [65–67] or graphene [68–71].

The second main approach has employed some form of bosonization [26–33,72–81]. By means of a Hubbard-Stratonovich transformation [82,83], the fermionic system with a pointlike interaction can be rewritten in terms of one or several "collective" bosons coupled to fermions by Yukawa couplings. For the microscopic pointlike interaction one can employ a standard form of the momentum dependence for the fermion-boson coupling, reflecting the properties of the corresponding channel. At this stage, the boson propagator is simply a constant. As the flow proceeds to smaller momentum scales, the inclusion of fluctuation effects generates a momentum dependence of the boson propagators. Furthermore, the bosonic part of the effective action does not remain quadratic in the boson fields. A nontrivial effective potential develops for these fields. A minimum of the potential at nonzero

field value indicates spontaneous symmetry breaking, with the corresponding order parameter given by the value of the bosonic field at the minimum of the potential. The flow can be followed into the ordered phase, and the divergences in the four-fermion vertex at the onset of local order can be avoided. This has allowed to establish antiferromagnetic and d-wave superconducting order in corresponding regions of parameter space [24–33], and the existence of competing order [33].

An important aspect of the bosonized approach is the possibility of "dynamic bosonization" [73–78]. Fluctuations generate four-fermion interactions even if the original pointlike four-fermion interaction has been bosonized via a Hubbard-Stratonovich transformation and replaced by boson-fermion interactions. Flowing bosonization allows to (partially) absorb the newly generated four-fermion vertex in the flow of the propagator and the Yukawa couplings of the interacting system of fermions and bosons. Using dynamical bosonization, there is no need to start with a Hubbard-Stratonovich transformation. One may keep the fermionic interaction, and only attribute dominant fluctuation effects to a suitable boson exchange [32,33].

Both approaches have their advantages and disadvantages. The purely fermionic description allows for a detailed and unbiased resolution of the momentum dependence of the four-fermion vertex. No *a priori* guess on relevant channels is necessary. The disadvantage is a rather indirect description of spontaneous symmetry breaking. Typically, the quartic four-fermion vertex diverges at the onset of local spontaneous symmetry breaking, and the flow cannot be continued reliably into the ordered phase.

In contrast, a bosonic description is well suited for a description of spontaneous symmetry breaking. The effective potential develops terms that are quartic in the bosonic fields. Such a potential can account for spontaneous symmetry breaking whenever the term quadratic in the boson fields, the boson "mass term," becomes negative. The vanishing of the mass term at the onset of spontaneous symmetry breaking produces the divergence of the four-fermion vertex in the corresponding purely fermionic description. Quartic boson interactions, which stabilize the effective potential, correspond to vertices with eight fermions in the purely fermionic language, which are hard to incorporate in the purely fermionic flow.

The disadvantage of bosonic methods is the necessity of guessing the relevant channels corresponding to collective bosons. In most applications, the remnant four-fermion interaction is dropped. Since the relevant channels may differ for different parameters of the macroscopic model, and several channels may be equally important, the guess introduces a certain bias in the description. For example, in mean-field theory results depend strongly on the choice of the channels in the Hubbard-Stratonovich transformation [28–30]. This dependence is greatly reduced once fluctuations of the collective bosons are included [84], but a residual bias remains for a given truncation (see, e.g., [85]). Furthermore, the exchange of collective bosons restricts the possible momentum dependence of the effective four-fermion interaction generated by the boson exchange. In a more physical sense, one has to guess what kind of order parameter could be realized in the vacuum state of the system and introduce the corresponding collective (auxiliary) fields. In other words, in this method, one has to guess in advance which symmetries are likely to be broken by the dynamics of electrons.

TABLE I. Comparison between different methods. The abbreviations are given as follows. (PF): pure fermionic theory; (HS): bosonization via the Hubbard-Stratonovich transformation without residual four-fermion interaction; (DB): dynamical bosonization without residual four-fermion interaction; (DBF): dynamical bosonization with residual four-fermion interaction; (SSB): naturally access to spontaneous symmetry breaking with order parameter; (FM): full momentum dependence of complete four-fermion vertex; (FL): fluctuations on all scales included for leading channels; (BF): free of bias of channel selection. The check mark (✓) indicates that a method can naturally address to an issue.

	SSB	FM	FL	BF
PF		✓		✓
HS	✓			
DB	✓		✓	
DBF	✓	✓	✓	✓

This has led to approaches that combine the introduction of resonant channel with the fermionic description: Within a purely fermionic description an organization of the momentum-dependent four-fermion interaction in terms of important collective channels has been advocated [20]. In QCD a Fiertz-complete basis of the four-fermion interaction has been taken into account, while treating the resonant scalar-pseudoscalar channel with dynamical bosonization [79,80]. Such a Fiertz-complete approach with full momentum dependence requires sophisticated numerical tools, and the numerics in this paper is based on the numerical tools developed in [79,80] for relativistic systems. The setup allows in particular to check whether or not additional channels are resonant. In QCD in the vacuum this is not the case and no competing order effects occur. For the Hubbard model, the problem of competing order parameters has been studied in Refs. [24,25] within an effective mean-field theory for the momentum modes that have not yet been included at the scale where the four-fermion vertex diverges. For investigations of competing order on the bosonized side the idea is to use only a partial bosonization, while keeping, in addition, a four-fermion interaction. This approach has been followed in [32,33], where a momentum-independent four-fermion interaction is kept in addition to the one generated by boson exchange. In Table I we summarise comparisons between different methods.

In this paper we propose to combine partial bosonization with a momentum-dependent residual four-fermion interaction. The flow of the four-fermion action can be followed by use of an N-patching scheme. We suggest a truncation that involves a combined system of fermions and bosons, for which the bosonic fields represent fermion bilinears or more complicated collective fields. We propose to keep a momentum-dependent four-fermion vertex in addition to the flow of boson propagators, Yukawa interactions, and an effective potential for the bosons. Partial bosonization can be employed to convert the four-fermion vertex into the exchange of collective bosons as much as possible. This approach preserves all the advantages of a bosonic description. In addition, the momentum resolution of the total four-fermion

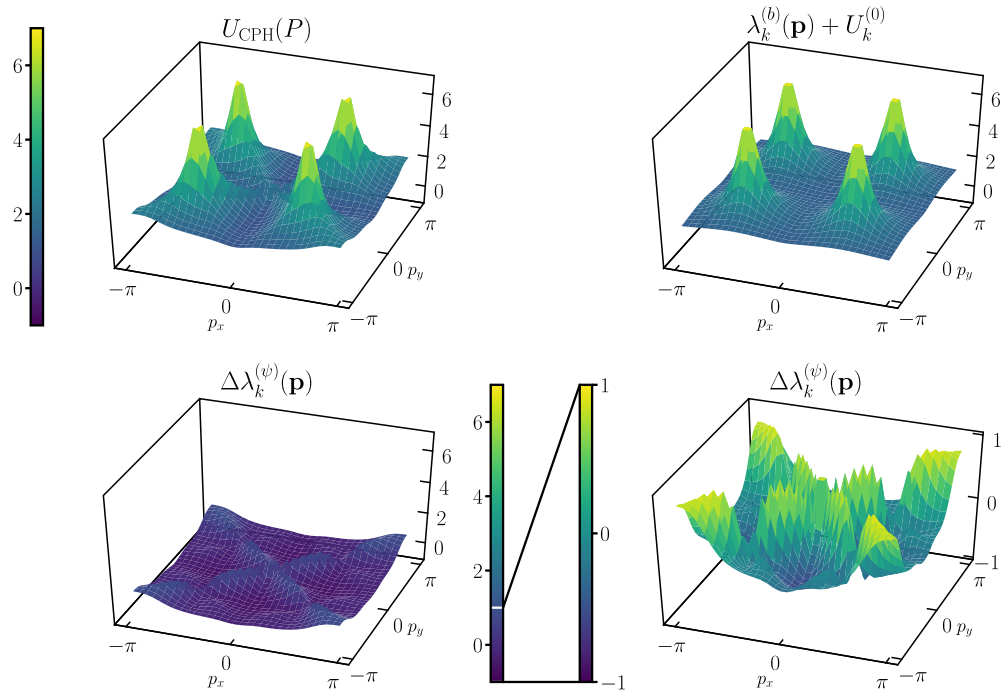

FIG. 1. Momentum dependence of the four-fermion vertex. Parameters are $\mu = t' = 0$, $U/t = 3$, $T = 0.1$, and the vertex is evaluated at $k_{\mathrm{IR}} \approx 0.9t$ ($T_k \approx 0.25t$). We display $U_k(P, P, -P, -P) = U_{\mathrm{CPH}}(P)$, where at one-loop level only the crossed particle-hole channel (CPH) contributes, with $P = (0, p_x, p_y)$. The top left panel shows the numerical result, which is dominated by nesting peaks located at $(\pm\pi/2, \pm\pi/2)$. The top right panel shows a boson-exchange mediated vertex of the form $\lambda_k^{(b)}(\boldsymbol{p}) + U_k^{(0)} = 2(m_k^2 + A_k[2\boldsymbol{p} - \boldsymbol{\pi}]^2)^{-1} + \lambda_k^{(0)}$, where m_k^2, A_k, and $\lambda_k^{(0)}$ are momentum-independent fitting parameters. The bottom panels show the momentum dependence of the residual four-fermion interaction, given by the difference between the two vertices on the top panels, $\Delta\lambda_k^{(\psi)}(\boldsymbol{p}) = U_{\mathrm{CPH}}(P) - [\lambda_k^{(b)}(\boldsymbol{p}) + U_k^{(0)}]$. The bottom right panel is a magnified version of the one on the bottom left. Differences between $U_{\mathrm{CPH}}(P)$ and $\lambda_k^{(b)}(\boldsymbol{p}) + U_k^{(0)}$ are overall about one order of magnitude smaller than the peaks.

interaction is no longer limited since it appears in the residual four-fermion interaction, which remains even after dynamical bosonization. There remains a residual bias in the selection of the channels in which boson fields are introduced. Only for these channels, higher-order terms in the bosonic fields can represent corresponding eighth-order fermionic interactions. The consequences of this bias are much reduced, however, since the momentum dependence of the residual four-fermion interaction can still "detect" important channels that may have been omitted by the guess for the bosonized channels.

A crucial ingredient for the proposed scheme of partial bosonization is the relative size of the boson-mediated and the residual four-fermion interaction. This is the focus of this paper. Partial bosonization is most efficient if the leading part of the full effective four-fermion interaction can be expressed in terms of boson exchanges, with a comparatively small residual four-fermion interaction. Here, we concentrate on the antiferromagnetic phase for which the exchange of bosons associated to antiferromagnetic spin waves is indeed found to be the dominant interaction.

The main result of this work is demonstrated in Fig. 1. The upper left figure shows the momentum dependence of the four-fermion vertex in an appropriate projection in the space of momenta of the fermions. It has been computed by solving the purely fermionic flow using the N-patching method down to a particular scale k_{IR}. At this scale we investigate to which extent the four-fermion vertex can be accounted for by boson exchange. The upper right plot displays the contribution of a boson exchange, expressed via a generic boson propagator with three fitted parameters. The residual four-fermion vertex after subtraction of the boson-exchange contribution is presented in the lower left. It is substantially smaller than the boson-exchange contribution, and shows less structure, as shown in the magnified plot in the lower right. All quantities are evaluated at a momentum scale k_{IR} of the flow close to the onset of local order. More details on this are given in Sec. II. This figure suggests that the four-fermion vertex is dominated by the exchange of a collective degree of freedom called antiferromagnetic boson. An investigation of other momentum channels confirms this picture. Combining three different momentum channels we find, in addition, indications for an s-wave pairing boson to play a role, being subleading as compared to the antiferromagnetic boson. All three-momentum channels are simultaneously well described by the exchange of antiferromagnetic and s-wave pairing bosons, together with a constant four-fermion interaction. The momentum dependence of the residual four-fermion interaction is found to be small.

This paper is organized as follows: In Sec. II we present our main findings by taking as a specific example a region in parameter space where antiferromagnetic order is expected. Section III specifies our notation for the Hubbard model and Sec. IV recapitulates the relevant features of functional renormalization. Section V describes the fermionic flow, and Sec. VI discusses partial bosonization. Finally, we summarize our findings in Sec. VII.

II. PARTIAL BOSONIZATION OF THE FOUR-FERMION INTERACTION

Partial bosonization has been employed to describe transitions in the effective degrees of freedom within the FRG. The main idea is to rewrite the "four-fermion vertex" or "two-particle vertex", or parts of it, in terms of exchanges of an antiferromagnetic boson:

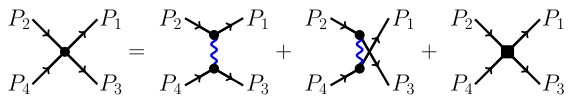

(1)

Here, the left-hand side is the four-fermion interaction given in the pure fermionic system. The first diagram on the right-hand side can be interpreted as an electron and a hole forming an "antiferromagnetic boson," which then decays into an electron and a hole again. The second diagram on the right-hand side accounts for electron-hole scattering by exchange of the antiferromagnetic boson. Finally, the third diagram on the right-hand side denotes the residual four-fermion vertex after the subtraction of the boson-exchange contribution from the full vertex. We can interpret this equation in both directions. We can either employ it to decompose a given vertex into a bosonic and a residual part. Or, in the bosonic formulation, it accounts for the full effective vertex in terms of contributions from boson exchange and an "irreducible" part. Formally, it constructs the connected four-point function from one-particle-irreducible (1PI) parts. Note in this context that in the purely fermionic language the total vertex is 1PI. There is some freedom in the choice of the split between boson exchange and residual four-fermion interaction, which can be used to optimize the procedure. Observable results, such as the gap in the fermion propagator due to collective order, have to be independent of the choice of the split. This can serve as a partial error estimate for a given approximation.

Dynamical bosonization provides for an exact formal method [73–78] of translating parts of the four-fermion interaction to an effective action for bosons and fermions. It can always be implemented. However, the crucial question is under which circumstances it is useful. If one keeps the momentum dependence of the residual four-fermion vertex, the addition of bosonic degrees of freedom and their interactions first adds to the complexity of the problem. Partial bosonization will only be useful if the most relevant parts of the four-fermion interaction are captured by the boson exchange, while it seems superfluous if the residual interaction dominates. The relative importance of the boson exchange is a quantitative question that we investigate here by solving the flow of the four-fermion interaction numerically, and by comparing the size of the boson exchange and the residual four-fermion interaction at the scale k_{IR}.

The central quantity for this problem is the four-fermion interaction [see Eq. (17) in Sec. III], which we parametrize by a momentum-dependent coupling $U_k(P_1, P_2, P_3, P_4)$. Here, P_i, $i = 1, \ldots, 4$, are the momenta and frequencies of the fermions in the vertex, and the index k indicates that we consider a scale-dependent coupling which flows from a microscopic scale to a macroscopic scale as the effects of fluctuations are successively incorporated. The corresponding term in the scale-dependent effective action (effective average action or coarse-grained free energy) Γ_k reads as

$$\Gamma_k^{\mathrm{int}} = \frac{1}{2}\sum_{P_i} \delta(P_1 - P_2 + P_3 - P_4)\, U_k(P_1, P_2, P_3, P_4) \times \psi_\alpha^\dagger(P_1)\psi_\alpha(P_2)\,\psi_\beta^\dagger(P_3)\psi_\beta(P_4), \tag{2}$$

where $P_i = (\omega, p_x, p_y)_i$ is the shorthand notation collecting the Matsubara frequency ω and a two-dimensional (2D) momentum $\boldsymbol{p} = (p_x, p_y)$ for the electron field ψ_α, where the indices α, β denote the electron spin. More concrete setups and definitions for the FRG and the Hubbard model are presented in the following sections. The initial value of U_k at the microscopic scale $k = \Lambda$ is given by the Hubbard coupling U for a pointlike interaction, which is a momentum-independent constant

$$U_\Lambda(P_1, P_2, P_3, P_4) = U, \tag{3}$$

with Λ of the order of the inverse lattice distance. Using the FRG equation with an N-patching scheme for the four-fermion vertex, we follow the RG flow of $U_k(P_1, P_2, P_3, P_4)$ from an ultraviolet (UV) scale $k = \Lambda$ to a certain infrared (IR) scale $k = k_{\mathrm{IR}}$. We do not resolve the frequency dependence here, working at $\omega_i = 0$. For a general momentum configuration, $U_{k_{\mathrm{IR}}}(P_1, P_2, P_3, P_4)$ is then a nontrivial function of three independent two-dimensional momenta.

Partial bosonization should capture the nontrivial momentum dependence of $U_k(P_1, P_2, P_3, P_4)$ in terms of boson-exchange processes. Let us add to the effective action a bosonic part

$$\Gamma_k^a = \sum_{Q,j}\left\{\frac{1}{2}\phi_j(-Q)\big(\hat{G}_k^{(a)}(Q)\big)^{-1}\phi_j(Q) - \sum_{P_1,P_2}\delta(Q - P_1 + P_2)\psi_\alpha^\dagger(P_1)(\sigma^j)_{\alpha\beta}\psi_\beta(P_2)\phi_j(Q)\right\}. \tag{4}$$

The three boson fields $\phi_j(Q)$ correspond to the Fourier modes of spin waves in the spin-one channel, with σ^j the Pauli matrices. For the particular momentum $Q = \Pi = (0, \pi, \pi)$, this is an antiferromagnetic spin wave. The inverse propagator of a boson of this type is taken to be

$$\big(\hat{G}_k^{(a)}(Q)\big)^{-1} = m_k^2 + A_k[Q - \Pi]^2, \tag{5}$$

with $[P]^2 = p_x^2 + p_y^2$ if $p_x, p_y \in [-\pi, \pi]$, and periodically continued outside the Brillouin zone. The superscript (a) denotes the"antiferromagnetic" type boson. It is chosen to have its minimum at $Q = \Pi$ if $A_k > 0$. A nonzero expectation value $\langle\phi_j(Q = \Pi)\rangle$ corresponds to antiferromagnetic order. The Yukawa coupling of the bosons to the electrons is set to one here.

The field equation for ϕ_j in the presence of fermion fields reads as

$$\phi_j(Q) = \sum_{P_1}\hat{G}_k^{(a)}(Q)\psi^\dagger(P_1)\sigma^j\psi(P_1 + Q). \tag{6}$$

This identifies ϕ_j with a fermion bilinear. A Gaussian integration over the boson field amounts to insertion of the field

equation (6) into the effective action Γ_k^a, resulting in

$$\Gamma_k^a = -\frac{1}{2}\sum_j \sum_{Q,P_1,P_3} \hat{G}_k^{(a)}(Q)[\psi^\dagger(P_1)\sigma^j\psi(P_1-Q)] \times [\psi^\dagger(P_3)\sigma^j\psi(P_3+Q)]. \tag{7}$$

With the identity

$$\sum_j (\sigma^j)_{\alpha\beta}(\sigma^j)_{\gamma\delta} = 2\delta_{\alpha\delta}\delta_{\beta\gamma} - \delta_{\alpha\beta}\delta_{\gamma\delta}, \tag{8}$$

the boson-exchange contributions to U_k in Eq. (2) lead to the term

$$\lambda_k^{(a)} = 2\hat{G}_k^{(a)}(P_2-P_3) + \hat{G}_k^{(a)}(P_1-P_2). \tag{9}$$

This procedure corresponds to the inversion of the Hubbard-Stratonovich transformation. The two terms can be associated with two boson-exchange processes. Either one electron with momentum $\boldsymbol{p}_2$ and a hole with momentum $-\boldsymbol{p}_3$ can form a boson with momentum $\boldsymbol{q} = \boldsymbol{p}_2 - \boldsymbol{p}_3$. Or, two electrons with momenta $\boldsymbol{p}_2$ and $\boldsymbol{p}_4$ are scattered to two electrons with momenta $\boldsymbol{p}_1$ and $\boldsymbol{p}_3$, with momentum transfer $\boldsymbol{q} = \boldsymbol{p}_1 - \boldsymbol{p}_2$ carried by the exchanged boson, and similar for hole-hole scattering. We may represent the two processes graphically by

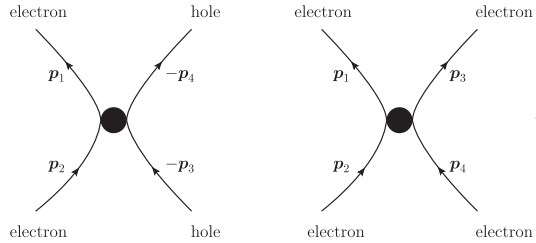

(10)

According to the momentum conventions in Eq. (2), the spin is conserved along each line. These graphs already account for the reordering of spin indices according to Eq. (8). They are different from the Feynman graphs for which the boson-fermion vertex involves σ^j.

The residual four-fermion interaction after subtraction of the boson-exchange contribution is given by

$$\lambda_k^{(\psi)} = U_k - \lambda_k^{(a)}, \tag{11}$$

where the superscript (ψ) stands for the residual pure four-fermion interaction corresponding to the last term on the right-hand side of Eq. (1). We are interested in the relative size of $\lambda_k^{(\psi)}$ as compared to $\lambda_k^{(a)}$. More precisely, we compare the momentum-dependent part $\Delta\lambda_k^{(\psi)}$ of $\lambda_k^{(\psi)}$ to U_k, subtracting a momentum-independent part:

$$\Delta\lambda_k^{(\psi)}(P_i) = \lambda_k^{(\psi)}(P_i) - U_k^{(0)}. \tag{12}$$

The constant part $U_k^{(0)}$ could also be incorporated in $\lambda_k^{(a)}$, where it would amount to an additive constant in the propagator $\Delta\hat{G}_k^{(a)} = U_k^{(0)}/3$. It seems natural, however, to keep it as part of the residual four-fermion interaction $\lambda_k^{(\psi)}$ as in Refs. [32,33].

As an example of a momentum configuration of the four-fermion coupling, we take the momentum configuration $(P_1, P_2, P_3, P_4) = (P, P, -P, -P)$, which corresponds to the "crossed particle-hole" channel in accordance with [20,86]. For this configuration we obtain

$$\lambda_k^{(a)}(P) = \frac{2}{m_k^2 + A_k[(2p_x-\pi)^2 + (2p_y-\pi)^2]} + \frac{1}{m_k^2 + 2\pi^2 A_k}. \tag{13}$$

The upper left part in Fig. 1 shows $U_{\mathrm{CPH}}(P) = U_k(P, P, -P, -P)$ with $P = (0, p_x, p_y)$ as a function of (p_x, p_y). We observe pronounced peaks of $U_k(p_x, p_y)$ at $(p_x, p_y) = (\pm\pi/2, \pm\pi/2)$. At these values of the momenta one has $[(2p_x-\pi)^2 + (2p_y-\pi)^2] = 0$, such that $\lambda_k^{(a)}(p_x, p_y)$ has a maximum. The upper right part in Fig. 1 shows $\lambda_k^{(a)}(p_x, p_y)$. We find good agreement with $U_k(p_x, p_y)$; the four-fermion vertex is indeed well described by a boson exchange. In order to determine m_k^2 and A_k, we have performed a three-parameter fit of U_k with the ansatz

$$U_k(\boldsymbol{p}) = \lambda_k^{(a)}(\boldsymbol{p}) + U_k^{(0)} = 2(m_k^2 + A_k[2\boldsymbol{p} - \boldsymbol{\pi}]^2)^{-1} + \lambda_k^{(0)}. \tag{14}$$

At $k_{\mathrm{IR}} \approx 0.9t$ we find

$$m_k^2 = 0.32, \qquad A_k = 0.53, \qquad U_k^{(0)} = 1.08. \tag{15}$$

The second part in Eq. (13) only contributes a small part to the constant $\lambda^{(0)}$ obtained from the fit,

$$\lambda_k^{(0)} - U_k^{(0)} = \frac{1}{m_k^2 + 2\pi^2 A_k} = 0.09. \tag{16}$$

The residual four-fermion interaction $\Delta\lambda_k^{(\psi)} = U_k - \lambda_k^{(b)} - U_k^{(0)}$ is displayed in the lower left panel of Fig. 1.

Other momentum configuration cases will be investigated in Sec. VI (see Figs. 2 and 3). The results support the overall effectiveness of partial bosonization. In the following sections, we introduce our setups for the Hubbard model and the FRG and then explain in a more concrete way how we fit the boson-exchange contributions to $U_{k_{\mathrm{IR}}}(P_1, P_2, P_3, P_4)$.

III. HUBBARD MODEL

The Hubbard model describes nonrelativistic fermions on a lattice, e.g., as a toy model for electrons in Mott insulators. For a 2D square lattice, the microscopic action of the single-band fermionic Hubbard model in momentum space is given by

$$S(\psi^\dagger, \psi) = \sum_Q \psi_\alpha^\dagger(Q)(i\omega_Q + \xi_{\boldsymbol{q}})\psi_\alpha(Q) + \frac{U}{2}\sum_{P_i} \psi_\alpha^\dagger(P_1)\psi_\alpha(P_2)\psi_\beta^\dagger(P_3)\psi_\beta(P_4) \times \delta(P_1 - P_2 + P_3 - P_4). \tag{17}$$

Here, we have introduced the shorthand notations $Q := (\omega_Q, \boldsymbol{q}) \equiv (\omega_Q, q_x, q_y)$ and

$$\delta(P-Q) := \frac{(2\pi)^2}{T}\delta(\omega_P - \omega_Q)\delta^{(2)}(\boldsymbol{p}-\boldsymbol{q}),$$
$$\sum_Q := T\sum_{n\in\mathbb{Z}} \int_{-\pi}^{\pi} \frac{d^2q}{(2\pi)^2}. \tag{18}$$

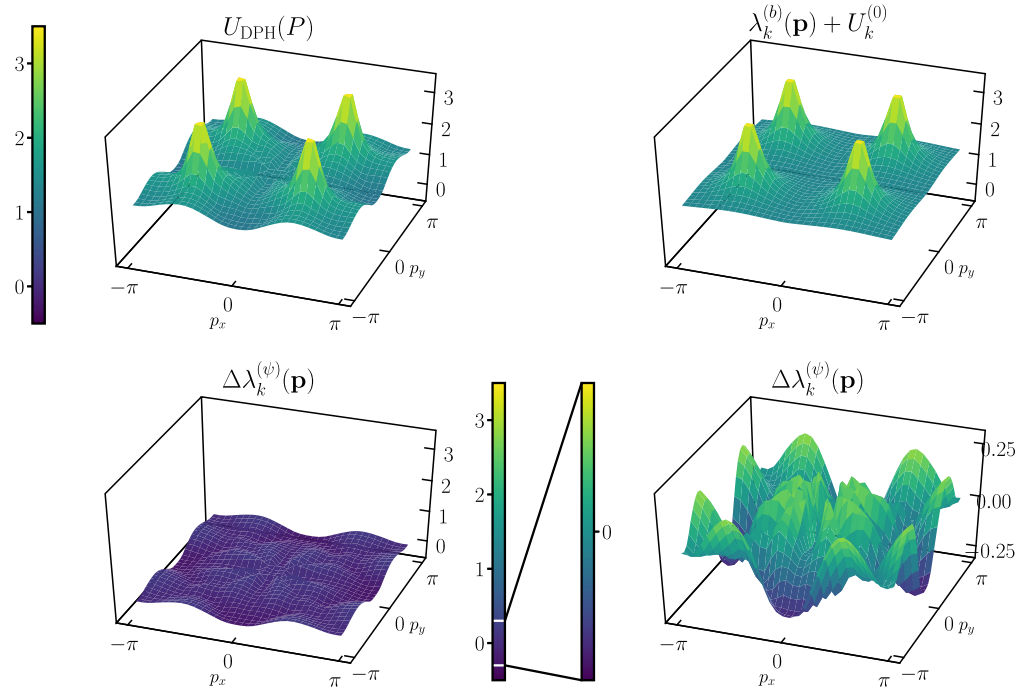

FIG. 2. Four-fermion coupling $U_k(P, -P, -P, P) = U_{\mathrm{DPH}}(P)$, $P = (0, p_x, p_y)$, where at one-loop level only the direct particle-hole channel (DPH) contributes. Parameters are the same as for Fig. 1. The numerical result shown in the top left panel is dominated by nesting peaks located at $(\pm\pi/2, \pm\pi/2)$. The top right panel shows a bosonic-exchange propagator of the form $\lambda^{(b)}_{\mathrm{DPH}}(\boldsymbol{p}) + U_k^{(0)} = (m_k^2 + A_k[2\boldsymbol{p} - \boldsymbol{\pi}]^2)^{-1} + \lambda^{(0)}_{\mathrm{DPH}}$ fitted to the result. We find that $U_{\mathrm{DPH}}(P) \approx \lambda^{(b)}_{\mathrm{DPH}}(\boldsymbol{p}) + U_k^{(0)}$ to high accuracy. The bottom panels show the the momentum dependence of the residual four-fermion vertex as difference between $U_{\mathrm{DPH}}(P)$ and $\lambda^{(b)}_{\mathrm{DPH}}(\boldsymbol{p}) + U_k^{(0)}$, where the bottom right panel is a zoomed-in version of the one on the bottom left. Differences between $U_{\mathrm{DPH}}(P)$ and $\lambda^{(b)}_{\mathrm{DPH}}(\boldsymbol{p}) + U_k^{(0)}$ are overall about one order of magnitude smaller than the peaks.

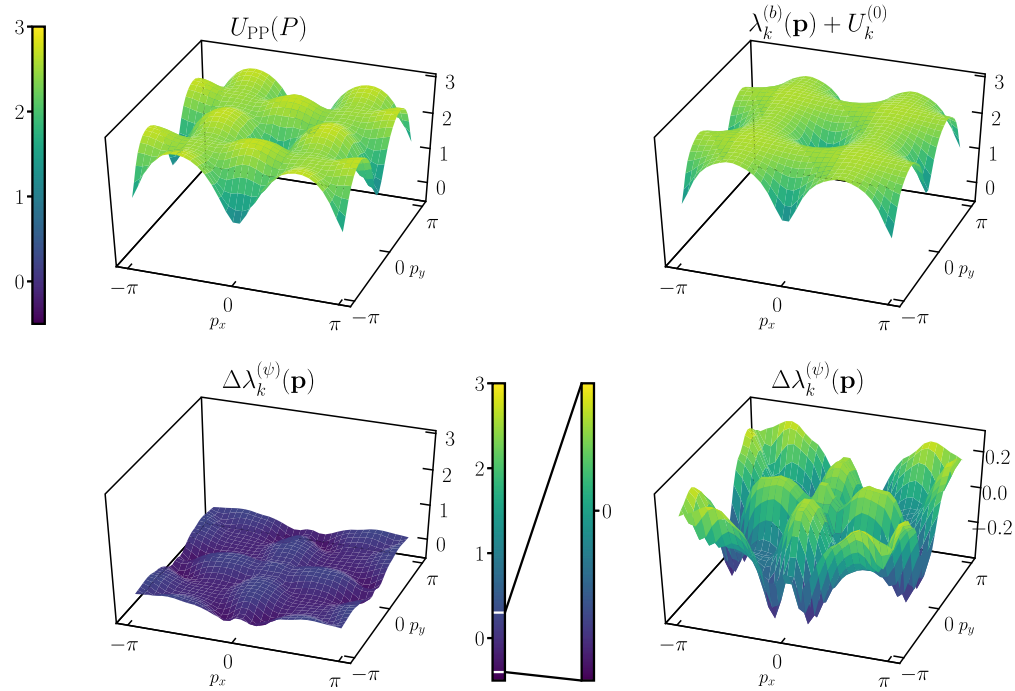

FIG. 3. Four-fermion coupling $U_k(P, P, P, P) = U_{\mathrm{PP}}(P)$, $P = (0, p_x, p_y)$, where at one-loop level only the particle-particle channel (PP) contributes. The numerical result shown in the top left panel is qualitatively different from the one in the particle-hole channels. Instead of nesting peaks, we observe a suppression of U_k at $p_x = 0, \pm\pi$ and $p_y = 0, \pm\pi$. The top right panel shows a bosonic-exchange propagator of the form $\lambda^{(b)}_{\mathrm{PP}}(\boldsymbol{p}) + U_k^{(0)} = (m_k^2 + A_k[2\boldsymbol{p}]^2)^{-1} + \lambda^{(0)}_{\mathrm{PP}}$ fitted to the result. We find that $U_{\mathrm{PP}}(P) \approx \lambda^{(b)}_{\mathrm{PP}}(\boldsymbol{p}) + U_k^{(0)}$ is a good approximation. The bottom panels show the difference between $U_{\mathrm{PP}}(P)$ and $\lambda^{(b)}_{\mathrm{PP}}(\boldsymbol{p}) + U_k^{(0)}$, where the bottom right panel is a zoomed-in version of the one on the bottom left. We find that differences between $U_{\mathrm{PP}}(P)$ and $\lambda^{(b)}_{\mathrm{PP}}(\boldsymbol{p}) + U_k^{(0)}$ are much smaller than the peaks.

The fermionic fields

$$\psi(Q) = (\psi_\uparrow(Q), \psi_\downarrow(Q))^T \tag{19}$$

describe fermions (electrons) on a square lattice which follow the momentum-space dispersion relation

$$\xi_{\boldsymbol{q}} = -\mu - 2t[\cos(q_x) + \cos(q_y)]. \tag{20}$$

Here, t denotes the the nearest-neighbor hopping parameters, and μ is the chemical potential associated with the doping level. In this work, we do not take into account the next-to-nearest-neighbor hopping. The fermionic Matsubara frequencies at a finite temperature T are given by $\omega_Q = 2\pi(n_Q + \frac{1}{2})T$. All components of the generalized momentum Q are measured in units of the lattice spacing a, i.e., $\boldsymbol{q} \to \boldsymbol{q}/a$. In this work, we always set $a = 1$.

The action (17) is invariant under global U(1) and SU(2) rotations. The U(1) symmetry corresponds to charge (or particle number) conservation, while the SU(2) symmetry reflects the spin-rotation invariance of the system. In addition, the Hubbard model is invariant under simultaneous rescalings of the imaginary time τ and the corresponding inverse rescalings of the parameters U, T, and t. For this reason, we express these quantities in units of the nearest-neighbor hopping t and consequently set $t = 1$ most of the time. Our numerical results employ $\mu = 0$, $T = 0.1$, and $U/t = 3$.

The energy dispersion relation $\epsilon_{\boldsymbol{q}} = \mu + \xi_{\boldsymbol{q}}$ satisfies the nesting property, i.e.,

$$\epsilon_{\boldsymbol{q}+\boldsymbol{\pi}} = -\epsilon_{\boldsymbol{q}}, \tag{21}$$

where $\boldsymbol{\pi} = (\pi, \pi)$ is the nesting vector. In particular, for $\mu = 0$ the half-filled band is realized and the fermion surface becomes a perfect square, the so-called umklapp surface. In this case the particle-hole channels are strongly enhanced. More specifically, for the momentum configurations $\boldsymbol{p}_1 - \boldsymbol{p}_2 = \pm\boldsymbol{\pi}$ and $\boldsymbol{p}_1 - \boldsymbol{p}_4 = \pm\boldsymbol{\pi}$, quantum fluctuations corresponding to bubbles of electron-hole pairs become strong, so that antiferromagnetic ordering (electron-hole condensate) takes place for any $U > 0$. We discuss this in more detail in Sec. V B.

IV. FUNCTIONAL RENORMALIZATION GROUP

In this section, we introduce the functional renormalization group (FRG). We then make an ansatz for the effective average action in order to solve the FRG equation. In this work, we take into account only the flow of the four-fermion interaction. We also describe our choice of the fermion regulator.

A. Flow equation

The FRG is a formulation of Wilson's RG in the context of quantum field theory. According to Wilson, renormalization should be thought of as a sequence of coarse-graining steps, each corresponding to integrating out quantum fluctuations in an infinitesimal momentum shell $k - \delta k < p < k$, where k denotes an IR cutoff scale. This process can be formulated as a functional differential equation for a scale-dependent effective action without any approximation. In this work, we employ the exact flow equation for the scale-dependent one-particle-irreducible (1PI) effective action (or effective average action) Γ_k [87], which reads as

$$\partial_k \Gamma_k = \frac{1}{2}\,\mathrm{Tr}\left[\frac{1}{\Gamma_k^{(2)} + R_k}\,\partial_k R_k\right]. \tag{22}$$

Here, Tr denotes a generalized functional trace over field space and all internal spaces such as frequencies, momenta, and spins. $\Gamma_k^{(2)}$ stands for the matrix of second functional derivatives of Γ_k with respect to the fields, i.e., the inverse propagator. The regulator R_k implements the coarse-graining within momentum integrations of Eq. (22) such that low-momentum modes $p < k$ are suppressed, and thus only high-momentum modes $p > k$ are effectively integrated out. In other words, the regulator in particular has to satisfy the conditions

$$\lim_{k\to 0} R_k(p) = 0, \qquad \lim_{k\to\Lambda\to\infty} R_k(p) = \infty. \tag{23}$$

The first condition implies that for $k \to 0$ one obtains the fully dressed effective action $\Gamma_{k=0} = \Gamma$. From the fact that the regulator behaves as a mass term for a finite IR scale k, the second condition is needed to suppress all quantum fluctuations in the high-energy limit, so that the initial condition for the flow is given by fixing the microscopic action S at the UV scale $k = \Lambda$, i.e., $\Gamma_\Lambda = S$. For more details on the FRG and its applications, see e.g. Refs. [75,86,88–92].

B. Effective average action

Although the flow equation (22) is exact, it generally cannot be solved exactly. In general, the effective action Γ_k obeying the flow equation (22) involves an infinite number of effective operators compatible with the symmetries of the theory. Therefore, we need to truncate our theory space in order to be able to do computations in practice. To this end, we make an ansatz for the effective action Γ_k and choose suitable projections to describe its flow in terms of flowing couplings. Here, we make the simple ansatz

$$\Gamma_k = \sum_Q \psi_\alpha^\dagger(Q)\tilde{P}_k^{\mathrm{f}}(Q)\psi_\alpha(Q) + \frac{1}{2}\sum_{P_i} U_k(P_1, P_2, P_3, P_4) \times \psi_\alpha^\dagger(P_1)\psi_\alpha(P_2)\,\psi_\beta^\dagger(P_3)\psi_\beta(P_4)\delta(P_1 - P_2 + P_3 - P_4), \tag{24}$$

where $\tilde{P}_k^{\mathrm{f}}(Q) = i\,\omega_Q + \xi_{\boldsymbol{q}}$ is the inverse fermion propagator, with ω_Q the Matsubara frequency and $\xi_{\boldsymbol{q}}$ the dispersion given in Eq. (20). In addition to the cutoff scale, the four-fermion coupling constant in the effective action (24) depends on external momenta.

C. Fermion regulator

There are various possible choices for the regulator $R_k^{\mathrm{f}}(Q)$ which obey the conditions (23). Here, we focus on the fact that the finite-temperature effect avoids the existence of zero modes in the fermionic propagator, i.e., $\omega_Q = \pi T$ for $n = 0$. Hence, the temperature itself plays the role of a regulator. For fermions we thus use an effective temperature cutoff [29,30]

$$R_k^{\mathrm{f}}(Q) = i\omega_Q\left(\frac{T_k}{T} - 1\right) = 2\pi i\left(n + \frac{1}{2}\right)(T_k - T). \tag{25}$$

With this cutoff, the temperature T in the Matsubara frequency is replaced by the scale-dependent effective temperature T_k. Here a general class of the scale-dependent effective temperature T_k is given by

$$(T_k)^p = T^p + \left(\frac{k^2}{\pi}\right)^p, \tag{26}$$

with p an integer larger than 2. In the long-wavelength limit $k^2 \ll T$, the fermionic effects should be suppressed in order for the bosonic picture to be relevant. For this reason, p has to be a sufficiently large value. In this work, we choose $p = 4$, for which the scale-dependent effective temperature is given as

$$T_k = \left[T^4 + \left(\frac{k^2}{\pi}\right)^4\right]^{\frac{1}{4}}. \tag{27}$$

For $k^2 \gg T$, one has $T_k \approx k^2/\pi$, such that the regulated inverse propagator behaves as $P_k \approx i(2n+1)k^2 + \xi_{\boldsymbol{q}}$, so that the zero mode is regulated by k^2, while for $k^2 \ll T$ the finite temperature πT regulates the zero mode. This is compatible with the fact that in nonrelativistic systems the lowest order of the kinetic energy is proportional to $\boldsymbol{p}^2$, namely, one can interpret the behavior $T_k \sim k^2$ for $k^2 \gg T$ as a regularization of the kinetic term of the fermionic field. Our numerical results are near $T = 0$ where $T_k \approx k^2/\pi$.

V. FLOW OF THE FOUR-FERMION COUPLING

In this section we present the flow equation of the four-fermion vertex and our approach to solving it. In addition, we investigate the resulting momentum dependence of the four-fermion coupling in the IR in the purely fermionic setting.

Using the flow equation (22) and projecting onto the momentum-dependent four-fermion coupling $U_k(P_1, P_2, P_3, P_4)$ in the effective action (24), we obtain the beta function

$$\partial_k U_k(P_1, P_2, P_3, P_4) = \mathcal{T}_{\mathrm{PP}} + \mathcal{T}_{\mathrm{DPH}} + \mathcal{T}_{\mathrm{CPH}}, \tag{28}$$

where "PP," "DPH," and "CPH" denote the particle-particle, direct particle-hole, and crossed particle-hole channel, respectively. We present the details of our projection scheme and the explicit forms of the flow diagrams $\mathcal{T}_i$ in Appendix A. At the initial scale $k = \Lambda$, we set the four-fermion coupling to a constant, i.e., $U_\Lambda(P_1, P_2, P_3, P_4) = U$. The flow equations hold for arbitrary temperature T. Our numerical results are evaluated at $T = 0.1$.

A. N patching and frequency dependence

The four-fermion vertex U_k is a function of four generalized momenta $P_i = (\omega_i, \boldsymbol{p}_i)$, each consisting of a Matsubara frequency ω_i and a two-dimensional momentum $\boldsymbol{p}_i$, giving a dependence on 12 parameters in total. Conservation of energy and momentum allows us to eliminate one generalized momentum, e.g., P_4, which, however, still leaves us with nine parameters in total. To further reduce the computational effort of our study, we thus make use of two main simplifications, which we explain in the following.

In the low-energy limit the most relevant effects would come from the dynamics of electrons on the Fermi surface. In other words, it is expected that the scaling dimensions of the four-fermion couplings with external energies and momenta perpendicular to the Fermi surface are negative at the fixed point associated to the antiferromagnetic phase transition, i.e., these couplings are irrelevant parameters in the sense of Wilson's RG, while the couplings corresponding to tangential external momenta are relevant parameters. Hence, as a first approximation, we neglect the external frequency dependence of the four-fermion coupling. This makes it possible to analytically perform the Matsubara sums occurring in the flow diagrams on the right-hand side of Eq. (28). We show the explicit computations in Appendix B.

In addition, we approximate the momentum dependence of the four-fermion vertices occurring on the right-hand side of Eq. (28) by projecting the two-dimensional momenta onto the Fermi surface, i.e.,

$$U_k(P_1, P_2, P_3, P_4) \approx U_k(\boldsymbol{p}_{1F}, \boldsymbol{p}_{2F}, \boldsymbol{p}_{3F}), \tag{29}$$

where $\boldsymbol{p}_{iF}$ denotes the projections of $\boldsymbol{p}_i$ onto the Fermi surface, and where we have explicitly used momentum conservation to eliminate $\boldsymbol{p}_4$. This allows us to still resolve the full momentum dependence of the four-fermion coupling in particular momentum channels, while significantly reducing computational effort by only feeding back a coupling depending on three parameters.

Furthermore, to numerically solve the flow of U_k in practice, we cannot evaluate U_k for continuous parameters, but instead employ a multidimensional grid of discrete parameters. In particular, we employ an N-patching scheme [14] for the four-fermion vertices fed back on the right-hand side of the flow equation of U_k. This is achieved by dividing the Brillouin zone into N patches for which momenta are parametrized by indices corresponding to the position of the patch, e.g., $\boldsymbol{p}_{1F} = \boldsymbol{p}_{n_1}$. All momenta in the same patch labeled by n_i are projected onto the same momentum on the Fermi surface, at the center of the patch. This way, in order to feed back the four-fermion vertex, we only need to keep track of a three-dimensional grid of couplings

$$U_k(\boldsymbol{p}_{1F}, \boldsymbol{p}_{2F}, \boldsymbol{p}_{3F}) \longrightarrow U_k(n_1, n_2, n_3). \tag{30}$$

The results presented in the following use $N = 24$.

B. Antiferromagnetic ordering

As mentioned in Sec. III, at half-filling with $\mu = 0$, antiferromagnetic ordering forms at sufficiently low temperature. A tendency to antiferromagnetism can be seen from the beta function for U_k. For the momentum configurations $\boldsymbol{p}_1 - \boldsymbol{p}_2 = \boldsymbol{\pi}$ (direct particle-hole channel) and $\boldsymbol{p}_1 - \boldsymbol{p}_4 = \boldsymbol{\pi}$ (crossed particle-hole channel), the kernel of threshold functions defined by $L_k(Q, Q-P) = \partial_k(G_k^{\mathrm{f}}(Q)G_k^{\mathrm{f}}(Q-P))$ does not depend on external momenta thanks to the nesting property (21), i.e., $L(Q, Q-P) = L(Q, Q)$. Within the N-patch approximation the dispersion (20) can be expanded around the Fermi surface,

$$\xi_{\boldsymbol{q}} \approx \xi_{\boldsymbol{q}_F} + \boldsymbol{v}_F|_{\boldsymbol{q}=\boldsymbol{q}_F} \cdot (\boldsymbol{q} - \boldsymbol{q}_F), \tag{31}$$

where $\boldsymbol{v}_F = \nabla_{\boldsymbol{q}}\xi_{\boldsymbol{q}}$ is the Fermi velocity. At half-filling one has $\epsilon_{\boldsymbol{q}_F} = \xi_{\boldsymbol{q}_F} + \mu = 0$. The saddle points $(\pm\pi, 0)$ and $(0, \pm\pi)$ have a vanishing Fermi velocity $\boldsymbol{v}_F = \boldsymbol{0}$ which causes the so-called van Hove singularities in the density of states. Another solution to $\boldsymbol{v}_F = \boldsymbol{0}$ is the nesting vector $\boldsymbol{\pi}$. Therefore, quantum fluctuations of particle-hole bubbles, $L(Q, Q)$, for the nesting external momenta enhance around the vanishing Fermi velocity $\boldsymbol{v}_F = \boldsymbol{0}$ because of the umklapp scattering with momentum transfer $\boldsymbol{\pi}$ and the nesting property. This strong enhancement is expected to generate antiferromagnetic order at sufficiently low T.

We present the results for U_k evaluated on the crossed and direct particle-hole channels, U_{CPH} and U_{DPH}, in Figs. 1 and 2. As can be seen in the top left plots of the figures, the particle-hole channels exhibit strongly enhanced peaks at momenta $\boldsymbol{p} = (\pm\pi/2, \pm\pi/2)$, which drive antiferromagnetic ordering effects. This behavior of the four-fermion coupling constant is driven by the umklapp and nesting processes mentioned above. We can interpret this as a signal for the breaking of SU(2) spin-rotation invariance in the system and as an emergence of antiferromagnetic ordering.

VI. PARTIAL BOSONIZATION

As explained in the last section, we integrate down the flow of the four-fermion coupling until we reach a scale close to the onset of antiferromagnetic ordering. There the divergence of nesting peaks in the particle-hole channels signals the transition to an antiferromagnetic phase, and we can no longer follow the flow of the four-fermion coupling in the purely fermionic setting. As discussed in Sec. V B, the nesting peaks are indeed the most prominent features in the particle-hole channels. In order to follow the flow of the four-fermion coupling into the symmetry-broken regime, we need to bosonize its corresponding channels.

In this section, we first present our results, which show that the nontrivial shape of the four-fermion coupling in different momentum channels can be well described by boson-exchange processes, parametrized by a few fitting parameters. After a short review of partial bosonization via the Hubbard-Stratonovich transformation, we explain our ansatz for the effective action to capture particle-hole or particle-particle scatterings in a bosonic language. We then attempt to bosonize the four-fermion coupling into an antiferromagnetic order boson and an additional boson which can be associated to s-wave Cooper pairing. We also investigate the shape and relative size of the residual four-fermion coupling.

A. Different momentum channels

In order to resolve the momentum dependence of the four-fermion coupling in more detail, we concentrate on three specific momentum channels, for which we employ two-dimensional grids of discrete momenta $P = (0, \boldsymbol{p})$ with $\boldsymbol{p} = (p_x, p_y)$. In particular, we investigate the momentum dependence of the four-fermion coupling for the following momentum configurations:

$$\begin{aligned} U_{\mathrm{CPH}}(P) &:= U_k(P, P, -P, -P), \\ U_{\mathrm{DPH}}(P) &:= U_k(P, -P, -P, P), \\ U_{\mathrm{PP}}(P) &:= U_k(P, P, P, P). \end{aligned} \tag{32}$$

TABLE II. Numerical results for fitting the ansatz (33) in different momentum configurations. An exchange of an antiferromagnetic boson a leads to a momentum-dependent contribution to the particle-hole channels, multiplied by the integer n_1, as well as a constant contribution in all three channels, multiplied by n_2. We can extract the fit parameters m_k^2 and A_k parametrizing the boson propagator from the momentum-dependent part, while the constant part together with an additional constant part of the four-fermion interaction $U_k^{(0)}$ leads to a total constant shift $\lambda_k^{(0)}$. Since an antiferromagnetic boson exchange only contributes an overall constant to the particle-particle channel, we cannot perform the same fit for this channel.

	(P_1, P_2, P_3, P_4)	$\lambda_k^{(b)}(n_1, n_2)$	m_k^2	A_k	$U_k^{(0)}$
CPH	$(P, P, -P, -P)$	$(2, 1)$	0.32	0.53	1.08
DPH	$(P, -P, -P, P)$	$(1, 2)$	0.41	0.69	1.08
PP	(P, P, P, P)	$(0, 3)$			

These momentum configurations have in common that for each of them specific channel momenta take a maximal value $2P$, namely, $P_{\mathrm{CPH}} := P_1 - P_4$, $P_{\mathrm{DPH}} := P_1 - P_2$, and $P_{\mathrm{PP}} := P_1 + P_3$, while many other sums or differences of momenta are zero. They can thus be associated to the crossed and direct particle-hole channels, and the particle-particle channel.

Boson exchanges affect the four-fermion vertex in different momentum channels differently. For example, the exchange of an antiferromagnetic boson contributes only a small constant in the particle-particle channel. With Eq. (9) the antiferromagnetic boson-exchange vertex is given by

$$\lambda_k^{(a)} = \frac{n_1}{m_k^2 + A_k[2\boldsymbol{p} - \boldsymbol{\pi}]^2} + \frac{n_2}{m_k^2 + 2\pi^2 A_k}, \tag{33}$$

with n_1 and n_2 integers, $n_1 + n_2 = 3$, given in Table II. The result of the fit for U_{DPH} is shown in Fig. 2, similar to the one for U_{CPH} in Fig. 1. The fitted parameters m_k^2, A_k, and $\lambda_k^{(0)}$ are shown in Table II.

In an ideal situation of a pure boson-exchange interaction, the same parameters m_k^2 and A_k should describe U_k for various momentum configurations. We observe that the values of m_k^2 and A_k extracted from the fits in the crossed and direct particle-hole channels are indeed of similar size, confirming the possibility of a partially bosonized description. In particular, Eq. (33) implies that the amplitude of the antiferromagnetic peaks in the CPH channel is twice the amplitude of the peaks in the DPH channel. This is approximately realized by the computed four-fermion interactions. For the peak locations P_0 we find $U_{\mathrm{CPH}}(P_0) \approx 6.87$, and $U_{\mathrm{DPH}}(P_0) \approx 3.46$. The absence of an antiferromagnetic enhancement in the PP channel is also realized by the computed four-fermion interaction, as we will see in more detail in Sec. VI E.

B. Bosonization of the four-fermion interaction

The exchange of an antiferromagnetic boson is not the only possibility. Other collective degrees of freedom, such as electron pairs [93], ferromagnetic bosons [94], or density waves [95] may play an important role in certain regions of the phase diagram of the Hubbard model. See also Refs. [29,32,33] in the context of partial bosonization. Each would contribute in specific momentum channels. Partial bosonization has to

account for all the various possibilities, as well as for interactions where two (or even more) collective modes play an important role.

Let us start with a short discussion of the basic notion of bosonization in a fermionic system. The Hubbard-Stratonovich transformation allows us to rewrite the purely fermionic action (17) as a Yukawa system such that

$$\begin{aligned} &S(\psi^\dagger, \psi, \phi) \\ &= \sum_Q \psi^\dagger(Q)(i\omega_Q + \xi_{\boldsymbol{q}})\psi(Q) + \frac{m^2}{2}\sum_Q \phi(-Q)\phi(Q) \\ &\quad - \sum_{P,Q} h[\psi^\dagger(P_1)\psi(P_2)\phi(Q)]\delta(Q - P_1 + P_2). \end{aligned} \tag{34}$$

At the level of the bare action, the (as of yet unspecified) bosonic field ϕ is an auxiliary field, i.e., a nondynamical field. The action (34) is equivalent to the pure fermionic action (17). Indeed, plugging the equation of motion for ϕ into the action (34), we get back the original action (17). The scalar boson mass parameter m^2 is related to the four-fermion coupling constant as

$$U = -\frac{h^2}{m^2}. \tag{35}$$

Here, the inverse scalar mass parameter is regarded as the momentum-independent propagator of the bosonic field. We can see explicitly that the Yukawa coupling can be eliminated by redefining the bosonic field $\phi \to \phi/h$ in the action (34), i.e., the Yukawa coupling h is a redundant coupling in the bare action. Hence, relation (35) implies that at the classical level the four-fermion vertex is rewritten in terms of an exchange process of the bosonic field, as diagrammatically represented in Eq. (1), although as of yet without external momentum dependencies or a residual four-fermion vertex.

The bosonic form (34) corresponds to the exchange of a density wave boson and leads to negative U. We can also use bosonization with an antiferromagnetic boson in the limit $A_k = 0$. In this case we obtain from Eq. (13)

$$U = \frac{3h^2}{m^2}. \tag{36}$$

The sign is opposite to the exchange of the density wave boson (35). There are further possibilities to perform bosonization along these lines, introducing a substantial amount of arbitrariness in the bosonization of a pointlike four-fermion interaction [29].

Fluctuation effects change the situation profoundly. They introduce a momentum dependence of U. Now, only particular choices of collective fields can generate by their exchange the dominant features of U, provided appropriate momentum-dependent bosonic propagators, and possibly momentum-dependent Yukawa interactions, are chosen.

For a half-filled lattice we expect the occurrence of antiferromagnetic ordering. The order parameter for this is $\langle\psi^\dagger\sigma^i\psi\rangle$, which characterizes the breaking of SU(2) spin-rotation symmetry. The collective modes corresponding to such an ordering are in the adjoint representation of SU(2), and we denote them by $m^i(Q)$ here. A typical feature associated to antiferromagnetic ordering is the occurrence of nesting peaks, for which the sum of incoming external momenta equals $\pm\boldsymbol{\pi}$. It is therefore useful for the description of antiferromagnetic ordering to introduce collective bosons with a constant shift in the momentum

$$a^i(Q) = m^i(Q + \Pi), \tag{37}$$

where $\Pi = (0, \boldsymbol{\pi})$. An expectation value of the antiferromagnetic boson a^i at zero momentum $\langle a^i(P = 0)\rangle \neq 0$ then corresponds to a homogeneous antiferromagnetic spin density.

C. Pairing bosons

In addition to the antiferromagnetic bosons a^i, we could introduce another collective mode corresponding to Cooper pairs of electrons, i.e., $\varphi \sim \langle\psi^T\varepsilon\psi\rangle$, with $\varepsilon = i\sigma^2$ the totally antisymmetric tensor. A nonvanishing expectation value of such a collective mode indicates the breaking of U(1) symmetry, which corresponds to charge conservation. This type of order is identified with a superconducting phase. To realize such a phase, however, the electrons should exhibit an effectively attractive force, for which a departure from half-filling may be crucial. Although Cooper pairing of electrons is not expected to occur in the system at half-filling, we may introduce a collective mode for Cooper pairing. Partial bosonization in two channels allows the exploration of more details of the four-fermion interaction and of other regions of the phase diagram.

So far we have encoded the particular momentum dependence of the boson-exchange-induced interaction in the ansatz for the boson propagator $\hat{G}$ [cf. Eq. (5)]. It is often more convenient, however, to account for this momentum dependence by an appropriate momentum-dependent form factor in the fermion-boson interaction. The inverse boson propagator can then be chosen to have its minimum at zero momentum, as for the antiferromagnetic boson a^i in Eq. (37). For the antiferromagnetic boson, the form factor consists of a shift of the boson momentum by Π. To avoid confusion, we will in the following refer to the propagators with the minima of their inverses fixed at $\boldsymbol{p} = 0$ as G instead of $\hat{G}$.

As a simple truncation for the effective action describing the bosonization of the four-fermion coupling in the antiferromagnetic or superconducting channels, we use

$$\begin{aligned} \Gamma_k = &\sum_Q \psi^\dagger(Q)(i\omega_Q + \xi_{\boldsymbol{q}})\psi(Q) + \Gamma_k^{\text{boson}} \\ &- \sum_{P_i,Q} h_{a,k}(P_1, P_2, Q)[\psi^\dagger(P_1)\sigma^i\psi(P_2)]a^i(Q) \\ &\times \delta(Q - P_1 + P_2 + \Pi) - \sum_{P_i,Q}\Delta\left(\frac{\boldsymbol{p}_1 - \boldsymbol{p}_2}{2}\right) \\ &\times h_{\varphi,k}(P_1, P_2, Q) \times ([\psi^T(P_1)\varepsilon\psi(P_2)]\varphi^*(Q) \\ &- [\psi^\dagger(P_1)\varepsilon\psi^*(P_2)]\varphi(Q)) \times \delta(P_1 + P_2 - Q). \end{aligned} \tag{38}$$

Here, a^i and φ are collective modes describing an antiferromagnetic spin wave and a general Cooper pair, respectively. We denote by $h_{a,k}$ and $h_{\varphi,k}$ the respective scale- and momentum-dependent Yukawa couplings. The square brackets denote spin-contracted fermion bilinears. The form factor $\Delta(\boldsymbol{p})$ specifies the momentum configuration of the Cooper

pairing. Depending on the state of the scattered electrons, the form factor can take the following forms:

$$\Delta(\boldsymbol{p}) = \begin{cases} 1 & (s \text{ wave}), \\ \frac{1}{2}[\cos(p_x) + \cos(p_y)] & (\text{extended } s \text{ wave}), \\ \frac{1}{2}[\cos(p_x) - \cos(p_y)] & (d_{x^2-y^2} \text{ wave}), \\ \sin(p_x)\sin(p_y) & (d_{xy} \text{ wave}). \end{cases} \tag{39}$$

For other possible form factors see, e.g., [95]. In particular, the $d_{x^2-y^2}$-wave configuration may be interesting for the understanding of an occurrence of the superconducting phase in strongly correlated systems since its form factor could describe an effectively attractive interaction between electrons. In this work, however, we do not specify the form factor since we would like to see whether and how well a boson-exchange process can capture the momentum dependence of the four-fermion coupling constant.

For the superconducting boson we may try a simple ansatz for the propagator similar to Eq. (5),

$$\left(G_k^{(\varphi)}(Q)\right)^{-1} = m_{\varphi,k}^2 + A_{\varphi,k}[Q]^2, \tag{40}$$

and take a momentum-independent Yukawa coupling $h_\varphi = 1$. The boson-exchange contribution to the four-fermion interaction is computed analogously to Sec. II. The solution to the field equation of φ reads as

$$\varphi(Q) = G_k^{(\varphi)}(Q) \sum_P \Delta\left(\boldsymbol{p} - \frac{\boldsymbol{q}}{2}\right) \psi_\alpha(P)\varepsilon_{\alpha\beta}\psi_\beta(Q-P), \tag{41}$$

with $\boldsymbol{q}$ the (spacelike) momentum component of Q. Insertion of this solution into the effective action induces the boson-exchange interaction

$$\Gamma_k^\varphi = \sum_{Q,P_i} G_k^{(\varphi)}(Q)\, \Delta\left(\boldsymbol{p}_1 - \frac{\boldsymbol{q}}{2}\right) \Delta\left(\boldsymbol{p}_2 - \frac{\boldsymbol{q}}{2}\right) \times\ \psi_\alpha^*(P_1)\varepsilon_{\alpha\beta}\psi_\beta^*(Q-P_1)\psi_\gamma(P_2)\varepsilon_{\gamma\delta}\psi_\delta(Q-P_2). \tag{42}$$

This can be brought into the form (2) by use of the identity

$$\varepsilon_{\alpha\beta}\varepsilon_{\gamma\delta} = \delta_{\alpha\gamma}\delta_{\beta\delta} - \delta_{\alpha\delta}\delta_{\beta\gamma}, \tag{43}$$

such that the boson-exchange contribution to U reads as

$$\lambda_k^{(\varphi)}(P_1, P_2, P_3, P_4) = -4G_k^{(\varphi)}(P_1 + P_3)\, \Delta\left(\frac{\boldsymbol{p}_3 - \boldsymbol{p}_1}{2}\right) \Delta\left(\frac{\boldsymbol{p}_4 - \boldsymbol{p}_2}{2}\right). \tag{44}$$

For the CPH channel with $(P, P, -P, -P)$, $P = (0, \boldsymbol{p})$, we have

$$\lambda_{\text{CPH}}^{(\varphi)}(P) = -4G_k^{(\varphi)}(0)\Delta^2(-\boldsymbol{p}). \tag{45}$$

In the DPH channel with $(P, -P, -P, P)$ we find $U_{\text{DPH}}^{(\varphi)}(P) = U_{\text{CPH}}^{(\varphi)}(P)$ since $\Delta(\boldsymbol{p}) = \Delta(-\boldsymbol{p})$. The PP channel with (P, P, P, P) yields a contribution

$$\lambda_{\text{PP}}^{(\varphi)}(P) = -4G_k^{(\varphi)}(2P)\Delta^2(0), \tag{46}$$

which vanishes for the $d_{x^2-y^2}$ and d_{xy} waves. For the s waves, $\Delta(0) = 1$.

D. Toward antiferromagnetism and superconductivity

This work is limited to an investigation of the validity of partial bosonization. It seems useful, nevertheless, to sketch our proposal for continuing the flow into the ordered phase, including parts of the parameter space for which superconductivity is expected. This proposal follows for the boson-exchange part [32,33], while we suggest to keep, in addition, a momentum dependent $\lambda_k^{(\psi)}$ instead of the constant used in Refs. [32,33]. For this purpose one will need an ansatz for Γ_k^{boson} in Eq. (38).

The bosonic part Γ_k^{boson} includes pure bosonic interactions involving the kinetic terms of a^i and d. We can parametrize it as

$$\Gamma_k^{\text{boson}} = \sum_X V_k(\alpha, \delta) + (\text{derivative terms}), \tag{47}$$

where the effective potential V_k in coordinate space-time $X = (t, \boldsymbol{x})$ is given by

$$V_k(\alpha, \delta) = m_{a,k}^2\, \alpha + m_{\varphi,k}^2 \delta + \frac{\lambda_{a,k}}{2}\alpha^2 + \frac{\lambda_{\varphi,k}}{2}\delta^2 + \cdots, \tag{48}$$

with $\alpha(X) = a^i(X)a^i(X)/2$ and $\delta(X) = \varphi^*(X)\varphi(X)$. This effective potential exhibits SU(2) (spin-rotation) symmetry.

Spontaneous symmetry breaking in the antiferromagnetic channel occurs if m_a^2 is negative for $k = 0$, or more precisely for k^{-1} of the order of the characteristic size of the probe. In this case, the mass parameter $m_{a,k}^2$ varies from a positive value to a negative one through zero. For $m_a^2(k = k_t) = 0$ the four-fermion interaction strength U_{k_t} diverges. This divergence, seen in many FRG investigations in the purely fermionic setting, indicates the onset of local symmetry breaking, typically with domain size k_t^{-1}. For a negative value of the mass parameter $m_{a,k}^2 < 0$, the effective potential has a minimum at nonzero field value. If this persists for $k \to 0$, this is a signal of antiferromagnetic ordering $\langle a^i \rangle = \langle \psi^\dagger \sigma^i \psi \rangle \neq 0$, as a consequence of SU(2) spin-rotation symmetry breaking.

For the derivative terms involving the kinetic terms of the bosonic fields a^i and φ, we could make several choices. A particularly simple choice amounts to assuming a separate and quadratic dependence on frequencies and momenta:

$$G_k^{-1}(Q) = Z_k \omega_Q^2 + A_k[\boldsymbol{q}]^2 + m_k. \tag{49}$$

Here, $[\boldsymbol{q}]^2 = \boldsymbol{q}^2$ if $\boldsymbol{q} \in [-\pi, \pi]^2$, and is periodically continued otherwise. Z_k and A_k are field renormalization factors. At the initial scale $k = \Lambda$, only the fermionic dynamics is relevant, so that we can infer $Z_\Lambda = A_\Lambda = 0$ as initial conditions. Positive finite values of Z_k and A_k would be generated by fluctuation effects in low-energy regimes, and then the bosonic field behaves as a dynamical collective mode.

Based on these general properties, we propose for the future a method for which explicit bosonic fields account for leading boson-exchange channels in the four-fermion interaction. The part $\lambda_k^{(b)}$ corresponding to these leading channels can be shifted to the bosonic sector at every scale k by dynamical bosonization [73–78]. The residual part $U_k^{(0)} + \Delta\lambda_k^{(\psi)}(P_1, P_2, P_3, P_4)$ should be kept in the truncation, with bosonic contributions adding to the fermionic fluctuation effects. The total four-fermion interaction U can then be

reconstructed as

$$U_k(P_1,P_2,P_3,P_4)=\lambda_k^{(b)}(P_1,P_2,P_3,P_4)+\Delta\lambda_k^{(\psi)}(P_1,P_2,P_3,P_4)+U_k^{(0)}. \tag{50}$$

The advantage of this method will be an enhanced resolution of the leading channels by taking into account the effective boson-potential (48) terms beyond the quadratic order. This procedure allows to explore the regions with local or global spontaneous symmetry breaking without being stopped by the divergence of the four-fermion interaction in a purely fermionic treatment.

E. Bosonization in different momentum channels

A given choice of bosonization is reflected in all different momentum channels. For example, in our approximation the antiferromagnetic boson exchange leads in the particle-particle channel with (P,P,P,P) to a momentum-independent constant. Subtracting this constant in the PP channel will not absorb much of the four-fermion interaction. This is demonstrated in Fig. 3. Indeed, $U_{\rm PP}(P)=U_k(P,P,P,P)$ does not exhibit the pronounced antiferromagnetic peaks visible in Figs. 1 and 2. It still shows some structure, which one may attribute to the exchange of other collective bosons.

In general, one may combine bosons in two or even more channels in order to account for the features in different momentum channels. The total four-fermion vertex U_k is then composed of different boson-exchange combinations $\lambda_k^{(i)}$, plus a residual contribution $\lambda_k^{(\psi)}$. We observe that some boson-exchange channels give negative contributions to U, as seen for the particle-pair bosons in Eq. (44) if the product of the form factors Δ is positive. Another negative contribution is due to density waves. Generalizing Eq. (34) by replacing m^2 with $(G_k^{(\rho)}(Q))^{-1}$ one finds a contribution to the four-fermion interaction

$$\lambda_k^{(\rho)}(P_1,P_2,P_3,P_4)=-G_k^{(\rho)}(P_2-P_1), \tag{51}$$

where we have again assumed $h_{\rho,k}=1$. The combination of attractive and repulsive contributions gives flexibility to the bosonization procedure, but makes it also sometimes difficult to disentangle different effects.

As an example, we may look at the PP channel with momenta (P,P,P,P). We observe in Fig. 3 a momentum structure very different from Figs. 1 and 2. If we want to associate this to boson-exchange peaks, we would need a negative contribution, similar to the exchange of density wave bosons or pairing bosons. With negative peaks at multiples of π we actually find a good fit for

$$U_k(P,P,P,P)=-4\big(m_k^2+A_k[2\boldsymbol{p}^2]\big)^{-1}+\lambda_{\rm PP}^{(0)}. \tag{52}$$

The factor 4 is somewhat arbitrary at this stage. It would correspond to the exchange of an s-wave or extended s-wave pairing boson according to Eq. (44), with the boson propagator (40).

To check the consistency of such a hypothesis, one has to look at the corresponding contribution in the CPH and DPH channels, for which the momentum dependence is given by the squared form factor in Eq. (45). For the s-wave pairing boson with $\Delta^2(-\boldsymbol{p})=1$ we obtain in these channels a constant contributing to $U_k^{(0)}$,

$$\Delta U_k^{(0)}=-\frac{4}{m_\varphi^2}\approx -1.66, \tag{53}$$

where we use the fit value from the PP channel $m_\varphi^2=2.41$. This would imply for the constant part not indicated by the exchange of the antiferromagnetic or pairing boson a value $U_{\rm CPH}^{(0)}\approx U_{\rm DPH}^{(0)}\approx 1.08+1.66=2.74$. This agrees reasonably well with the constant $U_{\rm PP}^{(0)}\approx 2.42$ extracted from the fit in the PP channel. We conclude that the simultaneous exchange of an antiferromagnetic and an s-wave pairing boson accounts for a reasonable fit of most of the momentum structures observed in all three investigated channels. Of course, in order to confirm such a hypothesis, other momentum channels should be explored as well.

If we replace the s wave by an extended s wave we would predict in the CPH and DPH channels an additional momentum dependence mediated by the exchange of the pairing boson

$$\lambda_{\rm CPH}^{(\varphi)}=\lambda_{\rm DPH}^{(\varphi)}=-\frac{1}{m_\varphi^2}[\cos(p_x)+\cos(p_y)]^2. \tag{54}$$

This should be visible in $\Delta\lambda_k^{(\psi)}(\boldsymbol{p})$ in Figs. 1 and 2 (lower right corner). The negative contribution is maximal for $p_x=p_y=0,\pm\pi$. This is not the observed structure, and we thus conclude that an extended s-wave boson does not play an important role. Our discussion exemplifies that the choice of appropriate bosons proceeds often by hypothesis and verification/falsification, rather than by a systematic treatment.

If we follow the hypothesis of a boson-exchange contribution from both an antiferromagnetic and s-wave pairing bosons we arrive in the three channels at a description of the four-fermion interaction by

$$U_{\rm CPH}(\boldsymbol{p})=2\,G_k^{(a)}(2\boldsymbol{p}+\boldsymbol{\pi})+c_k^{(a)}-\frac{4}{m_\varphi^2}+U_{\rm CPH}^{(0)}+\Delta\lambda_{\rm CPH}^{(\psi)}(\boldsymbol{p}),$$

$$U_{\rm DPH}(\boldsymbol{p})=G_k^{(a)}(2\boldsymbol{p}+\boldsymbol{\pi})+2c_k^{(a)}-\frac{4}{m_\varphi^2}+U_{\rm DPH}^{(0)}+\Delta\lambda_{\rm DPH}^{(\psi)}(\boldsymbol{p}),$$

$$U_{\rm PP}(\boldsymbol{p})=-4\,G_k^{(\varphi)}(2\boldsymbol{p})+3c_k^{(a)}+U_{\rm PP}^{(0)}+\Delta\lambda_{\rm PP}^{(\psi)}(\boldsymbol{p}), \tag{55}$$

with

$$c_k^{(a)}=G_k^{(a)}(\boldsymbol{\pi})=\frac{1}{m_{a,k}^2+2\pi^2A_{a,k}}. \tag{56}$$

Here, $G_k^{(a)}$ and $G_k^{(\varphi)}$ are both given by Eq. (40), but with different parameters m_k^2 and A_k.

For a fit to the four-fermion interaction at the scale $k_{\rm IR}$ we combine all constants to a common constant $\lambda_k^{(0)}$ and neglect $\Delta\lambda_k^{(\psi)}$. In each channel we therefore perform a fit with three parameters m_k^2, A_k, and $\lambda_k^{(0)}$. We obtain the following fit

parameters:

$$\begin{aligned}\left(m_k^2, A_k, \lambda_k^{(0)}\right)_{\mathrm{CPH}} &\approx (0.32, 0.53, 1.17),\\ \left(m_k^2, A_k, \lambda_k^{(0)}\right)_{\mathrm{DPH}} &\approx (0.41, 0.69, 1.22),\\ \left(m_k^2, A_k, \lambda_k^{(0)}\right)_{\mathrm{PP}} &\approx (2.41, 2.29, 2.68).\end{aligned} \tag{57}$$

The parameters m_k^2 and A_k should be similar for the CPH and DPH channels since both involve the same propagator $G_k^{(a)}$ for the antiferromagnetic boson. The parameters in the PP channel are different. In particular, we observe $m_{a,k}^2 \ll m_{\varphi,k}^2$, indicating that the antiferromagnetic channel dominates.

With the "measured values" $m_{i,k}^2, A_{i,k}, \lambda_{i,k}^{(0)}$ we can compute the residual constant part $U_k^{(0)}$ in the four-fermion interaction after subtraction of the constant boson-exchange contributions. From Eq. (55) one finds

$$U_{\mathrm{CPH}}^{(0)} \approx 2.76, \quad U_{\mathrm{DPH}}^{(0)} \approx 2.69, \quad U_{\mathrm{PP}}^{(0)} \approx 2.42. \tag{58}$$

The values are actually rather similar and close to three, indicating that at least for the considered channels the fluctuation contribution is dominated by boson exchange.

As can be seen in the upper right in Figs. 1 and 2, our fit works well in the particle-hole channels, where it captures the strong nesting peaks signifying the neighborhood of the onset of antiferromagnetic ordering quite nicely. In addition, the particle-particle channel exhibits a repulsive behavior, which can also be fitted by a s-wave pairing boson exchange, as shown in Fig. 3. The residual four-fermion interactions shown in the bottom of these figures are in all cases significantly smaller than the main features absorbed into the boson propagators. We also note that some of the differences could be artifacts stemming from the N-patching approximation we used to feed back the momentum dependence of the four-fermion coupling, or other truncation effects. In addition, if other effective boson-exchange processes like, e.g., a charge density wave played a role at half-filling, they should be visible in at least one of the channels we investigated. Since we observe no large additional contribution of this type, we can conclude that these processes as expected indeed do not play an important role in the transition to antiferromagnetic order, *a posteriori* justifying our ansatz for bosonizing the four-fermion coupling in Sec. VI D.

In summary, we find that the leading instabilities in the four-fermion interaction which signal the transition to antiferromagnetic order can be described as exchanges of an antiferromagnetic spin wave. While some substructures in the fermionic two-particle vertex are not absorbed by our simple bosonization ansatz, these are small compared to the nesting peaks in the particle-hole channels, and might at least partially be truncation artifacts. We thus conclude that it is indeed possible to bosonize the Hubbard model close to half-filling.

F. Buildup of bosonic-exchange channels

In order to investigate the buildup of antiferromagnetic ordering, we repeat the fits presented in Sec. VI E at different scales k, starting from the initial UV cutoff Λ (here $\Lambda = 6t$). We present the resulting scale dependence of the fit parameters m_k^2 and A_k in Fig. 4. As expected, close to the microscopic UV scale the values for m_k^2 and A_k are very large,

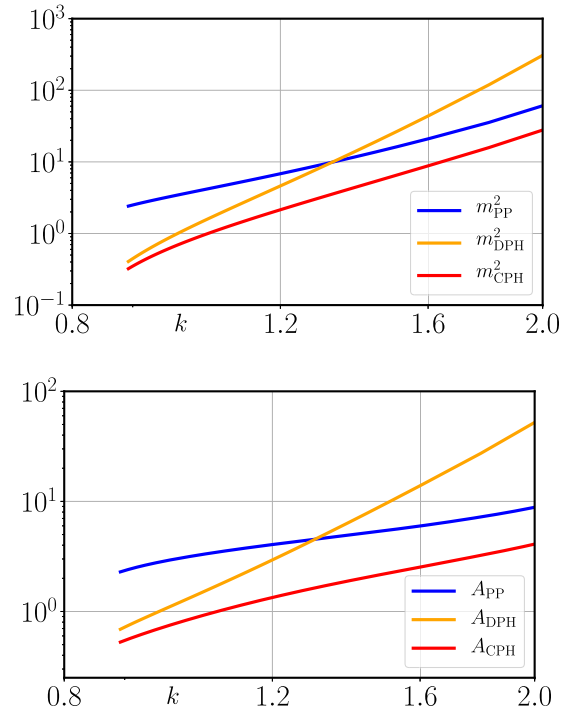

FIG. 4. Fit parameters m_k^2 and A_k for the boson-exchange propagators presented in Sec. VI E at different renormalization scales k. In all cases the values decrease exponentially toward the IR, signaling a buildup of nesting peaks, or more generally a nontrivial momentum dependence of the four-fermion coupling which can be described as an effective boson exchange. The parameters for the two particle-hole channels tend toward each other, consistent with the exchange of an antiferromagnetic boson in the two channels.

corresponding to a negligible boson-exchange contribution. The fit parameters become smaller toward the IR, however, signaling a buildup of nesting peaks in the particle-hole channels, and a nontrivial momentum dependence in the particle-particle channel. Close to the transition to antiferromagnetic ordering, where our flow stops numerically, the fit parameters for the particle-hole channels seem to flow toward the same values. We interpret this as a signal that the parts of the four-fermion interaction which signal the transition to antiferromagnetic order can indeed be bosonized by a single antiferromagnetic exchange boson a.

We also observe that for large k the effects of the exchange of antiferromagnetic and s-wave pairing bosons are of similar size. Only close to the onset of local antiferromagnetic order a clear dominance of the antiferromagnetic channel sets in.

VII. CONCLUSIONS

In this paper, we investigated the momentum dependence of the four-fermion coupling of the two-dimensional Hubbard model on a square lattice close to the transition to antiferromagnetic order. We found that the nesting singularities in the particle-hole channels driving the transition can be well described by the exchange of an antiferromagnetic spin wave. This already works for a particularly simple parametrization of the exchange-boson propagator. At half-filling the residual

four-fermion interaction is small compared to the part that can be described by boson exchange.

This suggests a split of the momentum-dependent four-fermion interaction U_k into a boson-exchange part $\lambda_k^{(b)}$, and a residual four-fermion interaction $\lambda_k^{(\psi)}$. This can be done at every scale k of the renormalization flow, i.e.,

$$U_k(P_i) = \lambda_k^{(b)}(P_i) + \lambda_k^{(\psi)}(P_i). \tag{59}$$

The boson-exchange part can be described by explicit bosonic fields for collective excitations using the method of flowing bosonization. Keeping a momentum-dependent residual interaction $\lambda_k^{(\psi)}$ is important in order to diminish the effects of a possible bias in the choice of the bosonization, maintain an accurate momentum dependence, and detect possible other channels for which U_k can get large, and which are not yet included in $\lambda_k^{(b)}$.

There is no need to restrict this method of partial bosonization to a single bosonic field. For two or more bosonic fields, effects of competing channels, competing order, or simultaneous order for several order parameters can be investigated. For the present investigation of three-momentum channels we find a good description of the momentum-dependent four-fermion vertex by the exchange of an antiferromagnetic and an s-wave pairing boson. The simultaneous flow of interactions for fermionic and bosonic degrees of freedom enhances the algebraic and numerical complexity. However, the bonus of access to the ordered phase and the increased resolution for the leading channels makes it worth it.

ACKNOWLEDGMENTS

We thank M. Scherer for discussions. This work is supported by EMMI, and is part of and supported by the Deutsche Forschungsgemeinschaft (DFG) Collaborative Research Centre SFB 1225 (ISOQUANT) as well as by the DFG under Germany's Excellence Strategy Grant No. EXC - 2181/1 - 390900948 (the Heidelberg Excellence Cluster STRUCTURES). M.Y. is supported by the Alexander von Humboldt Foundation.

APPENDIX A: FLOW EQUATION

In this Appendix, we show the explicit form of the beta function of the four-fermion coupling U_k occurring in the effective action (24). A key quantity in the flow equation is the two-point function $\Gamma_k^{(2)}$. In the Hubbard model, we compute the second-order functional derivative with respect to ψ and $\bar{\psi}$. Its result is shown in, e.g., [91]. In order to obtain the flow of U_k, we define the spin projector

$$\mathbb{P}_{s_1 s_2 s_3 s_4} = \tfrac{1}{2}\big(\delta_{s_1 s_2}\delta_{s_3 s_4} - \delta_{s_1 s_3}\delta_{s_2 s_4}\big). \tag{A1}$$

The flow equation of the four-fermion vertex U_k can then be obtained by acting with this projector on the flow equation of the four-point function. In summary, we arrive at

$$\partial_k U_k(P_1,P_2,P_3,P_4) = \mathrm{Tr}\left(\mathbb{P}\frac{\delta^4 \partial_k \Gamma_k}{\delta\psi(-P_4)\delta\psi^\dagger(P_3)\delta\psi(-P_2)\delta\psi^\dagger(P_1)}\right) = (\mathcal{T}_{\mathrm{PP}} + \mathcal{T}_{\mathrm{DPH}} + \mathcal{T}_{\mathrm{CPH}})\delta(P_1 - P_2 + P_3 - P_4), \tag{A2}$$

where we have used the flow equation (22) in the second line. The spin-projected flow diagrams $\mathcal{T}_i$ read as [20,96]

$$\begin{aligned}
\mathcal{T}_{\mathrm{PP}}(P_1,P_2,P_3,P_4) &= -\sum_Q L(-Q, Q+P_1+P_3) U_k(P_1,-Q,P_3,Q+P_1+P_3) U_k(-Q,P_2,Q+P_1+P_3,P_4),\\
\mathcal{T}_{\mathrm{DPH}}(P_1,P_2,P_3,P_4) &= -\sum_Q L(Q, Q+P_1-P_2)(-2U_k(P_1,P_2,Q,Q+P_1-P_2)U_k(Q+P_1-P_2,Q,P_3,P_4)\\
&\quad + U_k(P_1,Q+P_1-P_2,Q,P_2)U_k(Q+P_1-P_2,Q,P_3,P_4)\\
&\quad + U_k(P_1,P_2,Q,Q+P_1-P_2)U_k(P_3,Q,Q+P_1-P_2,P_4)),\\
\mathcal{T}_{\mathrm{CPH}}(P_1,P_2,P_3,P_4) &= -\sum_Q L(Q, Q-P_1+P_4) U_k(P_1,Q,Q-P_1+P_4,P_4) U_k(Q,P_2,P_3,Q-P_1+P_4).
\end{aligned} \tag{A3}$$

The abbreviations PP, DPH, and CPH stand for particle-particle, direct particle-hole, and crossed particle-hole channels, respectively, and we introduce the threshold function

$$L(P,Q) := \partial_k\big(G_k^{\mathrm{f}}(P)\, G_k^{\mathrm{f}}(Q)\big), \tag{A4}$$

with the full fermion propagator

$$G_k^{\mathrm{f}}(Q) = \frac{1}{i\,\omega_Q + \xi_{\boldsymbol{q}} + R_k^{\mathrm{f}}(Q)}. \tag{A5}$$

APPENDIX B: MATSUBARA-RESUMMED PROPAGATOR LOOPS

The flow generators (A3) involve Matsubara sums. In this work, as discussed in Sec. V, we approximate the four-fermion vertex as frequency independent and can therefore perform the Matsubara sums analytically. In particular, with $\omega_P = 2\pi T_k(n_P +$

$\frac{1}{2}) = \pm\omega_Q$, where $n_P \in \mathbb{Z}$ and the effective temperature cutoff (25), we obtain

$$T\sum_{n\in\mathbb{Z}} L(P,Q) = \partial_k\left(T\sum_{n\in\mathbb{Z}} G_k^{\mathrm{f}}(P)G_k^{\mathrm{f}}(Q)\right) = T\,\partial_k\left(-\frac{1}{2T_k}\frac{\tanh\left(\frac{\xi_p}{2T_k}\right)-\tanh\left(\frac{\xi_q}{2T_k}\right)}{\xi_p-\xi_q}\right),$$

$$T\sum_{n\in\mathbb{Z}} L(P,-Q) = \partial_k\left(T\sum_{n\in\mathbb{Z}} G_k^{\mathrm{f}}(P)G_k^{\mathrm{f}}(-Q)\right) = T\,\partial_k\left(\frac{1}{2T_k}\frac{\tanh\left(\frac{\xi_p}{2T_k}\right)+\tanh\left(\frac{\xi_q}{2T_k}\right)}{\xi_p+\xi_q}\right). \tag{B1}$$

We specified our choice of the fermion regulator and the precise form of the effective temperature T_k in Sec. IV C.

APPENDIX C: COMPUTATION CYCLE

We briefly summarize the computation cycle used in this paper.

(1) Derive beta functions by taking functional derivatives of exact flow equation.

(2) Solve the beta function of the four-fermion coupling $\partial_k U_k(P_1,P_2,P_3,P_4) = \mathcal{T}_{\mathrm{PP}} + \mathcal{T}_{\mathrm{DPH}} + \mathcal{T}_{\mathrm{CPH}}$ for three different momentum configurations (DPH, CPH, and PP) by using N-patching method. (The top left-hand side figures in Figs. 1–3.)

(3) We fit to the obtained $U_k(P_i) = U_k(P_1,P_2,P_3,P_4)$ in step 2 by the bosonic propagator

$$\lambda_k^{(b)}(P_i) = \frac{n_1}{m_k^2 + A_k[2\boldsymbol{p}-\boldsymbol{\pi}]^2} + \frac{n_2}{m_k^2 + 2\pi^2 A_k} + U_k^{(0)}, \tag{C1}$$

and find m_k^2, A_k, and $U_k^{(0)}$. (The top right-hand side figures in Figs. 1–3.)

(4) We evaluate the difference between $U_k(P_i)$ and $\lambda_k^{(b)}$,

$$\Delta\lambda_k^{(\psi)}(P_i) = U_k(P_i) - \lambda_k^{(b)}(P_i)\,. \tag{C2}$$

(The bottom hand side figures in Figs. 1–3.)

[1] J. G. Bednorz and K. A. Müller, Z. Phys. B: Condens. Matter **64**, 189 (1986).
[2] M. K. Wu, J. R. Ashburn, C. J. Torng, P. H. Hor, R. L. Meng, L. Gao, Z. J. Huang, Y. Q. Wang, and C. W. Chu, Phys. Rev. Lett. **58**, 908 (1987).
[3] P. W. Anderson, Science **235**, 1196 (1987).
[4] F. C. Zhang and T. M. Rice, Phys. Rev. B **37**, 3759 (1988).
[5] J. Hubbard, Proc. R. Soc. London, Ser. A **276**, 238 (1963).
[6] M. C. Gutzwiller, Phys. Rev. Lett. **10**, 159 (1963).
[7] J. Kanamori, Prog. Theor. Phys. **30**, 275 (1963).
[8] H. Tasaki, J. Phys.: Condens. Matter **10**, 4353 (1998).
[9] H. J. Schulz, Europhys. Lett. **4**, 609 (1987).
[10] P. Lederer, G. Montambaux, and D. Poilblanc, J. Phys. (Paris) **48**, 1613 (1987).
[11] I. Dzyaloshinskii, Sov. Phys.–JETP **66**, 848 (1987).
[12] I. Dzyaloshinskii, J. Phys. I **6**, 119 (1996).
[13] N. Furukawa, T. M. Rice, and M. Salmhofer, Phys. Rev. Lett. **81**, 3195 (1998).
[14] D. Zanchi and H. J. Schulz, Z. Phys. B: Condens. Matter **103**, 339 (1997).
[15] D. Zanchi and H. J. Schulz, Europhys. Lett. **44**, 235 (1998).
[16] C. J. Halboth and W. Metzner, Phys. Rev. Lett. **85**, 5162 (2000).
[17] C. J. Halboth and W. Metzner, Phys. Rev. B **61**, 7364 (2000).
[18] D. Zanchi and H. J. Schulz, Phys. Rev. B **61**, 13609 (2000).
[19] C. Honerkamp, Eur. Phys. J. B **21**, 81 (2001).
[20] M. Salmhofer and C. Honerkamp, Prog. Theor. Phys. **105**, 1 (2001).
[21] C. Honerkamp, M. Salmhofer, N. Furukawa, and T. M. Rice, Phys. Rev. B **63**, 035109 (2001).
[22] C. Honerkamp and M. Salmhofer, Phys. Rev. B **64**, 184516 (2001).
[23] A. A. Katanin and A. P. Kampf, Phys. Rev. B **72**, 205128 (2005).
[24] W. Metzner, J. Reiss, and D. Rohe, Phys. Status Solidi B **243**, 46 (2006).
[25] J. Reiss, D. Rohe, and W. Metzner, Phys. Rev. B **75**, 075110 (2007).
[26] H. C. Krahl, J. A. Müller, and C. Wetterich, Phys. Rev. B **79**, 094526 (2009).
[27] T. Baier, E. Bick, and C. Wetterich, Phys. Rev. B **62**, 15471 (2000).
[28] T. Baier, E. Bick, and C. Wetterich, arXiv:cond-mat/0107390.
[29] T. Baier, E. Bick, and C. Wetterich, Phys. Rev. B **70**, 125111 (2004).
[30] T. Baier, E. Bick, and C. Wetterich, Phys. Lett. B **605**, 144 (2005).
[31] H. C. Krahl and C. Wetterich, Phys. Lett. A **367**, 263 (2007).
[32] S. Friederich, H. C. Krahl, and C. Wetterich, Phys. Rev. B **81**, 235108 (2010).

[33] S. Singh, R. N. C. Pfeifer, and G. Vidal, Phys. Rev. B **83**, 115125 (2011).
[34] H. C. Krahl, S. Friederich, and C. Wetterich, Phys. Rev. B **80**, 014436 (2009).
[35] C. Husemann, K.-U. Giering, and M. Salmhofer, Phys. Rev. B **85**, 075121 (2012).
[36] K.-U. Giering and M. Salmhofer, Phys. Rev. B **86**, 245122 (2012).
[37] S. Uebelacker and C. Honerkamp, Phys. Rev. B **86**, 235140 (2012).
[38] A. Eberlein and W. Metzner, Phys. Rev. B **89**, 035126 (2014).
[39] J. Wang, A. Eberlein, and W. Metzner, Phys. Rev. B **89**, 121116(R) (2014).
[40] H. Yamase, A. Eberlein, and W. Metzner, Phys. Rev. Lett. **116**, 096402 (2016).
[41] C. Husemann and W. Metzner, Phys. Rev. B **86**, 085113 (2012).
[42] D. S. de la Peña, J. Lichtenstein, and C. Honerkamp, Phys. Rev. B **95**, 085143 (2017).
[43] D. Vilardi, C. Taranto, and W. Metzner, Phys. Rev. B **97**, 235110 (2018).
[44] K. Veschgini and M. Salmhofer, Phys. Rev. B **98**, 235131 (2018).
[45] C. J. Eckhardt, G. A. H. Schober, J. Ehrlich, and C. Honerkamp, Phys. Rev. B **98**, 075143 (2018).
[46] A. Tagliavini, C. Hille, F. B. Kugler, S. Andergassen, A. Toschi, and C. Honerkamp, SciPost Phys. **6**, 009 (2019).
[47] D. Vilardi, C. Taranto, and W. Metzner, Phys. Rev. B **99**, 104501 (2019).
[48] W. Metzner and H. Yamase, Phys. Rev. B **100**, 014504 (2019).
[49] M. Salmhofer, Nucl. Phys. B **941**, 868 (2019).
[50] J. E. Hirsch, Phys. Rev. B **31**, 4403 (1985).
[51] S. R. White, D. J. Scalapino, R. L. Sugar, E. Y. Loh, J. E. Gubernatis, and R. T. Scalettar, Phys. Rev. B **40**, 506 (1989).
[52] S. R. White, D. J. Scalapino, R. L. Sugar, N. E. Bickers, and R. T. Scalettar, Phys. Rev. B **39**, 839 (1989).
[53] A. Moreo, D. J. Scalapino, R. L. Sugar, S. R. White, and N. E. Bickers, Phys. Rev. B **41**, 2313 (1990).
[54] N. Bulut, Adv. Phys. **51**, 1587 (2002).
[55] A. Moreo, Phys. Rev. B **48**, 3380 (1993).
[56] R. Preuss, W. Hanke, and W. von der Linden, Phys. Rev. Lett. **75**, 1344 (1995).
[57] R. Preuss, W. Hanke, C. Gröber, and H. G. Evertz, Phys. Rev. Lett. **79**, 1122 (1997).
[58] D. Duffy, A. Nazarenko, S. Haas, A. Moreo, J. Riera, and E. Dagotto, Phys. Rev. B **56**, 5597 (1997).
[59] F. Krien, A. Valli, and M. Capone, Phys. Rev. B **100**, 155149 (2019).
[60] F. Krien and A. Valli, Phys. Rev. B **100**, 245147 (2019).
[61] G. V. Astretsov, G. Rohringer, and A. N. Rubtsov, Phys. Rev. B **101**, 075109 (2020).
[62] C. Taranto, S. Andergassen, J. Bauer, K. Held, A. Katanin, W. Metzner, G. Rohringer, and A. Toschi, Phys. Rev. Lett. **112**, 196402 (2014).
[63] A. Georges, G. Kotliar, W. Krauth, and M. J. Rozenberg, Rev. Mod. Phys. **68**, 13 (1996).
[64] U. Ellwanger and C. Wetterich, Nucl. Phys. B **423**, 137 (1994).
[65] F. Wang, H. Zhai, and D.-H. Lee, Europhys. Lett. **85**, 37005 (2009).
[66] F. Wang, H. Zhai, and D.-H. Lee, Phys. Rev. B **81**, 184512 (2010).
[67] F. Wang, H. Zhai, Y. Ran, A. Vishwanath, and D.-H. Lee, Phys. Rev. Lett. **102**, 047005 (2009).
[68] M. M. Scherer, S. Uebelacker, D. D. Scherer, and C. Honerkamp, Phys. Rev. B **86**, 155415 (2012).
[69] T. C. Lang, Z. Y. Meng, M. M. Scherer, S. Uebelacker, F. F. Assaad, A. Muramatsu, C. Honerkamp, and S. Wessel, Phys. Rev. Lett. **109**, 126402 (2012).
[70] M. M. Scherer, S. Uebelacker, and C. Honerkamp, Phys. Rev. B **85**, 235408 (2012).
[71] L. Classen, C. Honerkamp, and M. M. Scherer, Phys. Rev. B **99**, 195120 (2019).
[72] K.-I. Aoki, K. Morikawa, J.-I. Sumi, H. Terao, and M. Tomoyose, Phys. Rev. D **61**, 045008 (2000).
[73] H. Gies and C. Wetterich, Phys. Rev. D **65**, 065001 (2002).
[74] H. Gies and C. Wetterich, Phys. Rev. D **69**, 025001 (2004).
[75] J. M. Pawlowski, Ann. Phys. **322**, 2831 (2007).
[76] S. Floerchinger and C. Wetterich, Phys. Lett. B **680**, 371 (2009).
[77] J. Braun, L. Fister, J. M. Pawlowski, and F. Rennecke, Phys. Rev. D **94**, 034016 (2016).
[78] W.-j. Fu, J. M. Pawlowski, and F. Rennecke, Phys. Rev. D **101**, 054032 (2020).
[79] M. Mitter, J. M. Pawlowski, and N. Strodthoff, Phys. Rev. D **91**, 054035 (2015).
[80] A. K. Cyrol, M. Mitter, J. M. Pawlowski, and N. Strodthoff, Phys. Rev. D **97**, 054006 (2018).
[81] S. J. Wetzel, arXiv:1712.04297.
[82] R. L. Stratonovich, Dokl. USSR Academy of Sciences **115**, 1097 (1957) [Sov. Phys.–Dokl. **2**, 416 (1957)].
[83] J. Hubbard, Phys. Rev. Lett. **3**, 77 (1959).
[84] J. Jaeckel and C. Wetterich, Phys. Rev. D **68**, 025020 (2003).
[85] J. M. Pawlowski, M. M. Scherer, R. Schmidt, and S. J. Wetzel, Ann. Phys. **384**, 165 (2017).
[86] W. Metzner, M. Salmhofer, C. Honerkamp, V. Meden, and K. Schonhammer, Rev. Mod. Phys. **84**, 299 (2012).
[87] C. Wetterich, Phys. Lett. B **301**, 90 (1993).
[88] J. Berges, N. Tetradis, and C. Wetterich, Phys. Rep. **363**, 223 (2002).
[89] H. Gies, Lect. Notes Phys. **852**, 287 (2012).
[90] B. Delamotte, Lect. Notes Phys. **852**, 49 (2012).
[91] P. Kopietz, L. Bartosch, and F. Schütz, *Introduction to the Functional Renormalization Group*, Lecture Notes in Physics, Vol. 798 (Springer Nature, Switzerland AG, 2010), p. 1.
[92] J. Braun, J. Phys. G: Nucl. Part. Phys. **39**, 033001 (2012).
[93] S. Chakravarty, A. Sudbo, P. W. Anderson, and S. Strong, Science **261**, 337 (1993).
[94] W. von der Linden and D. M. Edwards, J. Phys.: Condens. Matter **3**, 4917 (1991).
[95] D. Scalapino, Phys. Rep. **250**, 329 (1995).
[96] P. Kopietz and T. Busche, Phys. Rev. B **64**, 155101 (2001).